applied sciences

MDPI

Article

Model-Assisted Reduced-Order ESO Based Command Filtered Tracking Control of Flexible-Joint Manipulators with Matched and Mismatched Disturbances

Changzhong Pan [1,2,*], Xiangyin Fei [1], Jinsen Xiao [3], Peiyin Xiong [1], Zhijing Li [1] and Hao Huang [1]

[1] School of Information and Electrical Engineering, Hunan University of Science and Technology, Xiangtan 411201, China
[2] School of Automation, Guangdong University of Petrochemical Technology, Maoming 525000, China
[3] Department of Mathematics, Guangdong University of Petrochemical Technology, Maoming 525000, China
* Correspondence: pancz@hnust.edu.cn

Abstract: Flexible-joint manipulators (FJMs) have been widely used in the fields of industry, agriculture, medical service, aerospace, etc. However, the FJMs in practical applications inevitably encounter various uncertainties including matched and mismatched disturbances. In this paper, we consider the high precision tracking control problem of FJMs in the presence of unknown lumped matched and mismatched disturbances. An efficient model-assisted composite control approach is proposed by integrating two reduced-order extended state observers (RESOs), a second-order command filtered backstepping (SCFB) technique and an error compensation dynamic system. Unlike some existing methods, the RESOs constructed with partial known model information are capable of estimating and compensating the matched and mismatched disturbances simultaneously. In addition, by employing the SCFB with an error compensation system, the proposed approach can not only overcome the problem of "explosion of complexity" inherent in backstepping, but also reduce the filtering errors arising from the command filters. The stability of the resulting control system and the convergence of error signals are guaranteed by Lyapunov stability theory. Comparative simulations are conducted for a single-link FJM with both matched and mismatched disturbances, and the results show that the proposed approach achieves a better tracking performance, i.e., compared with conventional backstepping method and adaptive fuzzy command filtered control method, the tracking accuracy is improved by 99.5% and 99.2%, respectively.

Keywords: flexible-joint manipulators; reduced-order extended state observer (RESO); backstepping; command filter; error compensation

Citation: Pan, C.; Fei, X.; Xiao, J.; Xiong, P.; Li, Z.; Huang, H. Model-Assisted Reduced-Order ESO Based Command Filtered Tracking Control of Flexible-Joint Manipulators with Matched and Mismatched Disturbances. *Appl. Sci.* **2022**, *12*, 8511. https://doi.org/10.3390/app12178511

Academic Editor: Alessandro Gasparetto

Received: 28 July 2022
Accepted: 22 August 2022
Published: 25 August 2022

1. Introduction

The last decades have witnessed a tremendous progress in the development of flexible manipulators. Roughly speaking, the flexible manipulators can be divided into flexible-link manipulators (FLMs) [1,2] and flexible-joint manipulators (FJMs) [3–5]. In this paper, we focus on the study of FJMs, whose joints are made up of harmonic reducer, torque sensor, and other elastic components. The FJMs usually exhibit many distinctive features, such as light weight, good flexibility, high human-robot interaction safety, etc. As a result, they have a wide application prospect in the fields of industry, agriculture, medical service, aerospace, and so on [6,7]. However, the flexible joints are easy to produce elastic vibrations during the movements, especially in high-speed operations, which greatly affect the control accuracy of FJMs. In addition, the model of FJMs in practical applications may contain various nonlinear uncertainties including matched and mismatched disturbances. If these uncertainties are ignored in the control design, the performances of the controllers will be deteriorated [8]. Therefore, the study on vibration suppression of FJMs in the presence of

uncertainties with a high precision control has attracted great attentions in both control theory and engineering community.

In the past decades, many effective control methods have been proposed for the control of FJMs, e.g., fuzzy control [9,10], singular perturbation control [11–13], feedback linearization control [14,15], backstepping control [16–19], etc. Among them, the backstepping control is a Lyapunov function-based recursive design method, which constructs control Lyapunov functions step by step and designs intermediate virtual control laws recursively until the actual control law is reached. However, it suffers from the drawback of "explosion of complexity", that is, the derivatives of virtual control laws designed in the procedures need to be computed repeatedly. To solve this problem, a dynamic surface control (DSC) was proposed in Ref. [20], where a first-order low-pass filter was introduced in each step to obtain the derivative of the virtual control law instead of taking the derivative directly. Based on the DSC technique, several adaptive control schemes [21–23] were proposed for the single-link FJMs with unknown nonlinearities, and a DSC backstepping-based impedance controller was designed in Ref. [24] for a 5-DOF flexible joint robot. However, these results do not consider the potential errors caused by the filters. Furthermore, the derivatives of virtual control laws in DSC are actually approximated through numerical differentiations, which may amplify the noise and reduce the control accuracy.

To avoid numerical differentiations, a second-order command filtered backstepping (SCFB) method was proposed in Refs. [25,26]. It obtains the derivatives of the virtual control laws through integrations instead of differentiations, which can not only avoid the problem of "explosion of complexity", but also simplify the controller design. With the SCFB technique, an adaptive neural tracking controller was designed in Ref. [27] for uncertain robotic manipulators, and an adaptive fuzzy controller was proposed in Ref. [28] for a two-link robotic manipulator. Furthermore, regarding the filtering errors produced by command filters, two improved SCFB controllers were designed in Refs. [29,30] for FJM systems, where two error compensation mechanisms were constructed to reduce the filtering errors. Unfortunately, most of the above mentioned methods do not consider the practical uncertainties that may exist in the control of FJMs.

To cope with uncertainties, intelligent control methods including neural networks (NNs) and fuzzy logic systems (FLSs), which are well-known for their universal approximation abilities, have been widely utilized for uncertain FJMs. For example, the uncertain model of FJMs was approximated by a Radial Basis Function (RBF) neural network in Ref. [31], on the basis of which an adaptive observer and DSC controller were developed. Similarly, an FLS was employed in Ref. [32] to approximate the unknown functions, and an adaptive fuzzy tracking controller was designed. However, both the NNs and the FLSs require complex online learning mechanisms, which are computationally expensive. Sliding mode control, which is famous for its insensitivity to uncertainties, has also been applied in the control of FJMs [33–36], but the phenomenon of chattering cannot be avoided.

Observer-based technique is an alternative to deal with uncertainties, which estimates the uncertainties by designing a state/disturbance observer. In Ref. [37], a high gain observer-based robust output feedback control approach was proposed for a single-link FJM with matched disturbances and parametric uncertainties. In Ref. [38], a nonlinear disturbance observer (NDO) based DSC approach was proposed for the FJM with input saturation and unknown nonlinear disturbance, where the NDO was applied to estimate the unknown external disturbance and compensate the saturation constrain. However, only matched disturbances were considered in these control methods. Extended state observer (ESO), which regards internal and external disturbances as an extended system state variable, is another effective and practical disturbance estimation and attenuation approach [39]. As for FJMs in the presence of disturbances, an ESO-based feedback linearization control method was proposed in Ref. [40], and a cascaded-ESO based sliding-model control strategy was proposed in Ref. [41]. However, the conventional ESO is only applicable for integral chain systems, which should satisfy the so-called matching conditions. Although the ESOs in Refs. [40,41] can transform a mismatched disturbance into a matched one, they

require a series of complex coordinate transformations, which make the control algorithms computationally complicated. In addition, the order of the constructed ESOs is greater than the system. For high-order systems like the FJM, it may bring about some negative effects of the high gain action, such as noise amplification and the peaking phenomenon [41].

Unlike conventional ESO, the reduced-order ESO (RESO) [42], which makes full use of the measurable system state information, can attenuate the peaking phenomenon and yield a better estimation performance. More importantly, the RESO can be applied to non-integral chain systems with matched and mismatched disturbances. Due to these advantages, the RESO has been widely used for the control of various engineering systems, such as missiles [43], gear-shifting actuators [44], underwater vehicles [45], DC-DC buck converters [46], all-clamped plates [47], etc. However, the application of RESO on FJMs has not been reported.

Based on the above literature review and analysis, it is noted that there are still many crucial problems worthy of being further investigated in the control of FJMs, which can be summarized as follows.

(1) The FJMs in practical applications inevitably encounter various uncertainties including matched and mismatched disturbances. Unfortunately, the current researches focus on the matched disturbances, while the mismatched ones are not considered. Although the conventional ESO can transform a mismatched disturbance into a matched one, it requires a series of complex coordinate transformations, which make the control algorithms computationally complicated;
(2) The backstepping technique employed for the control design of FJMs suffers from the drawback of "explosion of complexity". Although the DSC or SCFCB can deal with the computation problem, the potential errors caused by the introduction of filters are not considered, which may greatly reduce the tracking accuracy.

Motivated by the above considerations, this paper aims to propose an efficient model-assisted composite control approach for the high precision tracking control of FJMs in the presence of lumped matched and mismatched disturbances by integrating the techniques of RESO and the SCFB. More specifically, the uncertain model of a single-link FJM is first given, where all the uncertainties affecting the system including friction/damping terms and external disturbances are lumped as matched and mismatched disturbances. Then, two model-assisted RESOs are constructed to estimate the matched and mismatched disturbances in real time. On the basis of the estimation values from the RESOs, a feedback controller is derived by using the recursive backstepping methodology, where three second-order command filters (SCFs) are incorporated to overcome the problem of "explosion of complexity". In addition, an error compensation dynamic system is designed to reduce the filtering errors caused by the SCFs. By utilizing Lyapunov stability theory, it rigorously proves that all the error signals in the closed-loop control system are uniformly ultimately bounded, and converge to a small neighbourhood of the origin. Numerical simulations with comparisons to existing methods are finally presented to verify the effectiveness and efficiency of the proposed approach.

The novel features and main contributions of this paper are highlighted as follows.

(1) The RESOs constructed with partial known model information are capable of estimating and compensating the matched and mismatched disturbances simultaneously. This is much different from the existing ESO-based methods where complex coordinate transformations are required to convert a mismatched disturbance into a matched one. The developed control algorithm is thus robust and efficient;
(2) The inherent complexity problem of backstepping is addressed by employing the SCFB control, where the derivatives of the virtual control laws are obtained through integrations instead of differentiations. The transient control performance of the controller is thus improved;
(3) The potential filtering errors caused by the command filters are taken into account, and they are reduced by the error compensation dynamic system, which improves the steady-state tracking control accuracy.

The remainder of this paper is organized as follows. The dynamic model of a single-link FJM with disturbances and the corresponding control problem are presented in Section 2. The detailed control design including two RESOs, a backstepping controller, and an error compensation system is given in Section 3. The stability of the resulting control system is analysed in Section 4. Simulation results are presented in Section 5 to verify the effectiveness and efficiency of the proposed approach. The concluding remarks are finally discussed in Section 6.

2. Problem Formulation

This paper studies the control problem of an FJM with one flexible joint and one rigid link, whose physical model is shown in Figure 1.

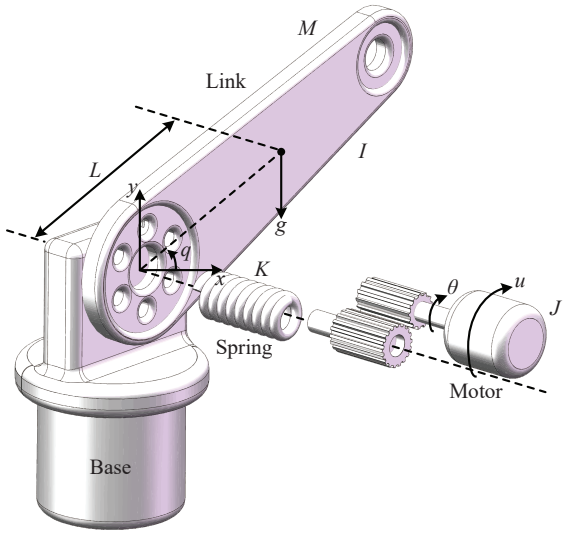

Figure 1. Physical model of a single-link FJM.

The parameters and variables in Figure 1 are given as follows: q and θ represent the angles of the link and the motor shaft, respectively; u is the control torque generated by the motor; g is the acceleration of gravity; M, K and L are the mass of the link, the spring stiffness of the flexible joint, the distance between the flexible joint, and the mass centre of the link, respectively; I and J are the rotational inertia of the rigid link and the motor, respectively.

According to the Euler–Lagrangian equation, the mathematical model of the single-link FJM is obtained as [16,48]:

$$\begin{cases} I\ddot{q} + K(q-\theta) + MgL\sin q = w_1 \\ J\ddot{\theta} - K(q-\theta) = u + w_2 \end{cases} \tag{1}$$

where w_1 and w_2 are the lumped disturbances including system friction/natural damping terms and unknown external disturbances.

Define $x = [x_1, x_2, x_3, x_4]^\top = [q, \theta, \dot{q}, \dot{\theta}]^\top$ as the state variable, and y as the output of the system, then the state-space equation of model (1) is written as:

$$\begin{cases} \dot{x}_1 = x_2 \\ \dot{x}_2 = x_3 + g_1(x) + d_1 \\ \dot{x}_3 = x_4 \\ \dot{x}_4 = \frac{1}{J}u + g_2(x) + d_2 \\ y = x_1 \end{cases} \tag{2}$$

where

$$\begin{aligned} g_1(x) &= -x_3 - \frac{K}{I}(x_1 - x_3) - \frac{MgL}{I}\sin x_1 \\ g_2(x) &= \frac{K}{J}(x_1 - x_3) \\ d_1 &= \frac{1}{I}w_1 \\ d_2 &= \frac{1}{J}w_2 \end{aligned} \tag{3}$$

Note that the terms $g_1(x)$ and $g_2(x)$ are straightforwardly derived from (1), and they are treated as nominal functions of the FJM model, which will be used for the control design. The main feature of the FJM system expressed as (2) is that it contains two terms d_1 and d_2, which are the mismatched and matched lumped disturbances, respectively. Generally speaking, the mismatched lumped disturbance d_1 is determined by the friction term and external disturbance, while d_2 represents the lumped disturbance caused by the natural damping and the disturbance generated by the control torque. In this paper, the mismatched and matched disturbances are simultaneously estimated by employing two RESOs, and the estimation values are fed back to the controller to compensate for their effects.

Considering the physical limitations on the FJM in practical applications, some assumptions are given as follows.

Assumption 1 ([30]). *The desired reference trajectory y_d and its first-order time derivative $\dot{y}_\mathrm{d}$ are available.*

Assumption 2 ([43]). *The lumped disturbances d_1, d_2, and their derivatives are all bounded, i.e., there exist positive constants $\bar{d}_1$, $\bar{d}_{1d}$, $\bar{d}_2$ and $\bar{d}_{2d}$ that satisfy $|d_1| \le \bar{d}_1$, $|\dot{d}_1| \le \bar{d}_{1d}$, $|d_2| \le \bar{d}_2$, $|\dot{d}_2| \le \bar{d}_{2d}$, $\forall t \in [0, +\infty)$.*

To facilitate the control design and stability analysis, the following lemmas are needed in the subsequent context.

Lemma 1 ([25]). *Consider the second-order command filters (SCFs) defined as*

$$\begin{cases} \dot{z}_i = z_{i\mathrm{d}} \\ \dot{z}_{i\mathrm{d}} = -2\zeta\omega_\mathrm{n} z_{i\mathrm{d}} - \omega_\mathrm{n}^2(z_i - \alpha_i) \end{cases} \quad (i = 1, 2, 3) \tag{4}$$

where α_i are the inputs and $\alpha_i^\mathrm{c} = z_i$, $\dot{\alpha}_i^\mathrm{c} = z_{i\mathrm{d}}$ are the outputs of the SCFs; ζ and ω_n are the damping ratio and bandwidth, respectively. Set the initial conditions as $z_i(0) = \alpha_i(0)$ and $z_{i\mathrm{d}}(0) = 0$. $\forall$ $t \ge 0$, if the inputs satisfy $|\dot{\alpha}_i| \le \varsigma_1$, $|\ddot{\alpha}_i| \le \varsigma_2$, where $\varsigma_1 > 0$, $\varsigma_2 > 0$, then there exist $\zeta \in (0, 1]$, $\omega_\mathrm{n} > 0$ and $\mu > 0$, such that $|z_i - \alpha_i| \le \mu$, $|z_{i\mathrm{d}} - \dot{\alpha}_i| \le \mu$, and $|\dot{z}_i|$, $|\ddot{z}_i|$, $|\dddot{z}_i|$ are bounded. Theoretically, the filtering errors of the SCFs can be made arbitrarily small by increasing ω_n.

The structure of an SCF is shown in Figure 2, from which it is clearly seen that the derivative of α_i is obtained through an integrator rather than a differentiator. This can reduce the measurement noise caused by differential operation and improve the control accuracy.

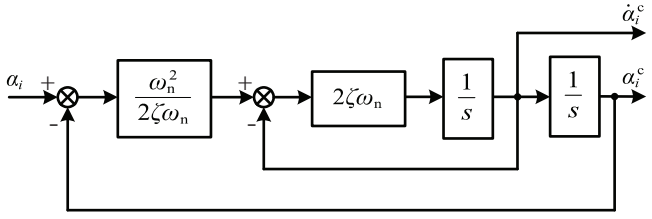

Figure 2. Structure of a second-order command filter.

Lemma 2 ([19,49]). *For $V : [0, +\infty) \in \mathbb{R}$, the solutions of inequality equations of $\dot{V}(t) \leq -aV(t) + f$ are*

$$V(t) \leq e^{-a(t-t_0)}V(t_0) + \int_{t_0}^{t} e^{-a(t-h)}f(h)dh, \ \forall t \geq t_0 \geq 0 \tag{5}$$

where a is any constant.

The control problem of this paper is formulated as following. Consider the single-link FJM (2) in the presence of lumped mismatched and matched disturbances. Design a proper controller by integrating the techniques of RESO and SCFB such that the output y tracks a desired trajectory y_{d} quickly and precisely.

3. RESO-Based Backstepping Control Design

To achieve the above control objective, in this section, two model-assisted RESOs are first designed to estimate the lumped matched and mismatched disturbances, and then a feedback controller with an error compensation mechanism is developed by employing the SCFB technique.

3.1. Reduced-Order ESO (RESO)

In order to estimate the lumped disturbances d_1 and d_2 in system (2), according to the design principle of RESO [42], two specified RESOs are given as

$$\begin{cases} \hat{d}_1 = p_1 + \beta_1 x_2 \\ \dot{p}_1 = -\beta_1 p_1 - \beta_1^2 x_2 - \beta_1 x_3 \end{cases} \tag{6}$$

$$\begin{cases} \hat{d}_2 = p_2 + \beta_2 x_4 \\ \dot{p}_2 = -\beta_2 p_2 - \beta_2^2 x_4 - \beta_2 J^{-1} u \end{cases} \tag{7}$$

where $\hat{d}_1$ stands for the estimate of the sum term of $g_1(x)$ and d_1; $\hat{d}_2$ stands for the estimate of the sum term of $g_2(x)$ and d_2; p_i and $\beta_i > 0 (i = 1, 2)$ are the auxiliary states and the observer gains, respectively.

Note that the internal dynamics $g_1(x)$ and $g_2(x)$ are available, which can be directly used as given model information for the observers. Hence, to reduce the estimation burden, the model-assisted RESOs are designed as

$$\begin{cases} \hat{d}_1 = p_1 + \beta_1 x_2 \\ \dot{p}_1 = -\beta_1 p_1 - \beta_1^2 x_2 - \beta_1 [x_3 + g_1(x)] \end{cases} \tag{8}$$

$$\begin{cases} \hat{d}_2 = p_2 + \beta_2 x_4 \\ \dot{p}_2 = -\beta_2 p_2 - \beta_2^2 x_4 - \beta_2 [J^{-1} u + g_2(x)] \end{cases} \tag{9}$$

where $\hat{d}_1$ and $\hat{d}_2$ stand for the estimates of the lumped uncertainties d_1 and d_2, respectively. Define the estimation errors as

$$\tilde{d}_1 = \hat{d}_1 - d_1 \tag{10}$$

$$\tilde{d}_2 = \hat{d}_2 - d_2 \tag{11}$$

Then, based on (8) and (10), the time derivative of $\tilde{d}_1$ can be obtained as

$$\begin{aligned} \dot{\tilde{d}}_1 &= \dot{\hat{d}}_1 - \dot{d}_1 = \dot{p}_1 + \beta_1 \dot{x}_2 - \dot{d}_1 \\ &= -\beta_1 p_1 - \beta_1^2 x_2 - \beta_1 [x_3 + g_1(x)] + \beta_1 [x_3 + g_1(x) + d_1] - \dot{d}_1 \\ &= -\beta_1 (p_1 + \beta_1 x_2) + \beta_1 d_1 - \dot{d}_1 \\ &= -\beta_1 \tilde{d}_1 - \dot{d}_1 \end{aligned} \tag{12}$$

According to the same derivation process, $\dot{\tilde{d}}_2$ can also be obtained as

$$\begin{aligned}\dot{\tilde{d}}_2 &= \dot{\hat{d}}_2 - \dot{d}_2 = \dot{p}_2 + \beta_2 \dot{x}_4 - \dot{d}_2 \\ &= -\beta_2 p_2 - \beta_2^2 x_4 - \beta_2[J^{-1}u + g_2(x)] + \beta_2[J^{-1}u + g_2(x) + d_2] - \dot{d}_2 \\ &= -\beta_2(p_2 + \beta_2 x_4) + \beta_2 d_2 - \dot{d}_2 \\ &= -\beta_2 \tilde{d}_2 - \dot{d}_2\end{aligned} \tag{13}$$

Combining (12) with (13), the disturbance estimation error dynamics for system (2) can be written in the following compact form:

$$\dot{\boldsymbol{e}}_o = \boldsymbol{A}_o \boldsymbol{e}_o + \dot{\boldsymbol{d}} \tag{14}$$

where $\boldsymbol{e}_o = [\tilde{d}_1,\ \tilde{d}_2]^{\mathrm{T}}$, $\dot{\boldsymbol{d}} = [-\dot{d}_1, -\dot{d}_2]^{\mathrm{T}}$ and $\boldsymbol{A}_o = \mathrm{diag}\{-\beta_1, -\beta_2\}$. Note that the gains in (8) and (9) are chosen as $\beta_i > 0 (i = 1, 2)$, which ensure that $\boldsymbol{A}_o$ is a Hurwitz matrix.

3.2. Second-Order Command Filtered Backstepping (SCFB) Controller

Based on the RESOs, a feedback tracking controller is designed by using the SCFB technique, and an error compensation system is proposed to reduce the filtering errors.

Firstly, we define the tracking errors as

$$\begin{cases} e_1 = y - y_{\mathrm{d}} \\ e_2 = x_2 - z_1 \\ e_3 = x_3 - z_2 \\ e_4 = x_4 - z_3 \end{cases} \tag{15}$$

where $z_i (i = 1, 2, 3)$ are the outputs of the SCFs defined in (4). In order to reduce the filtering errors produced by the SCFs, an error compensation dynamic system is designed as:

$$\begin{cases} \dot{\xi}_1 = -k_1 \xi_1 + \xi_2 + (z_1 - \alpha_1) \\ \dot{\xi}_2 = -\dfrac{1}{I} k_2 \xi_2 + \dfrac{K}{I}[\xi_3 + (z_2 - \alpha_2)] \\ \dot{\xi}_3 = -k_3 \xi_3 + \xi_4 + (z_3 - \alpha_3) \\ \dot{\xi}_4 = -k_4 \xi_4 \end{cases} \tag{16}$$

where $k_i > 0$ $(i = 1, 2, 3, 4)$ are design parameters, and the initial values of ξ_i $(i = 1, 2, 3, 4)$ are $\xi_i(0) = 0$. Then the compensated tracking errors are defined as

$$\begin{cases} v_1 = e_1 - \xi_1 \\ v_2 = e_2 - \xi_2 \\ v_3 = e_3 - \xi_3 \\ v_4 = e_4 - \xi_4 \end{cases} \tag{17}$$

Next, we derive the control laws to stabilize the tracking errors v_i by using the recursive backstepping methodology. The whole design procedure is divided into the following four steps.

Step 1: To stabilize v_1, the first Lyapunov function candidate is chosen as:

$$V_1 = \frac{1}{2} v_1^2 \tag{18}$$

Based on (2), (15) and (17), the time derivative of v_1 is computed by

$$\begin{aligned}\dot{v}_1 &= \dot{e}_1 - \dot{\xi}_1 = \dot{x}_1 - \dot{y}_{\mathrm{d}} - \dot{\xi}_1 \\ &= x_2 - \dot{y}_{\mathrm{d}} - \dot{\xi}_1 = v_2 + z_1 - \dot{y}_{\mathrm{d}} + \xi_2 - \dot{\xi}_1\end{aligned} \tag{19}$$

Taking the time derivative of V_1 along (19) and using the first equation of (16) yields

$$\begin{aligned}\dot{V}_1 &= v_1\dot{v}_1 = v_1\left(v_2 + z_1 - \dot{y}_\mathrm{d} + \xi_2 - \dot{\xi}_1\right)\\ &= v_1(v_2 + \alpha_1 - \dot{y}_\mathrm{d} + k_1\xi_1)\\ &= v_1(v_2 + \alpha_1 - \dot{y}_\mathrm{d} + k_1e_1 - k_1v_1)\end{aligned} \tag{20}$$

To make V_1 negative, the virtual control law α_1 is chosen as

$$\alpha_1 = -k_1e_1 + \dot{y}_\mathrm{d} \tag{21}$$

where k_1 is a positive design parameter. Substituting (21) into (20) yields

$$\dot{V}_1 = -k_1v_1^2 + v_1v_2 \tag{22}$$

Obviously, if $v_2 = 0$, then $\dot{V}_1 \leq 0$.

Step 2: Similarly, to stabilize v_2, the second Lyapunov function candidate is chosen as:

$$V_2 = V_1 + \frac{1}{2}Iv_2^2 \tag{23}$$

The time derivative of v_2 is obtained as

$$\begin{aligned}\dot{v}_2 &= \dot{e}_2 - \dot{\xi}_2 = \dot{x}_2 - \dot{z}_1 - \dot{\xi}_2\\ &= -\frac{K}{I}(x_1 - x_3) - \frac{1}{I}MgL\sin x_1 + d_1 - z_{1d} - \dot{\xi}_2\\ &= \frac{K}{I}(v_3 + z_2 + \xi_3) - \frac{K}{I}x_1 - \frac{1}{I}MgL\sin x_1 + d_1 - z_{1\mathrm{d}} - \dot{\xi}_2\end{aligned} \tag{24}$$

Taking the time derivative of V_2 along (24) and using the second equation of (16) yields

$$\begin{aligned}\dot{V}_2 &= \dot{V}_1 + Iv_2\dot{v}_2\\ &= -k_1v_1^2 + v_1v_2 + v_2\left[K(v_3 + z_2 + \xi_3) - Kx_1 - MgL\sin x_1 + Id_1 - Iz_{1\mathrm{d}} - I\dot{\xi}_2\right]\\ &= -k_1v_1^2 + v_2(v_1 + Kv_3 + K\alpha_2 - Kx_1 - MgL\sin x_1 + Id_1 - Iz_{1d} + k_2e_2 - k_2v_2)\end{aligned} \tag{25}$$

To make V_2 negative, the virtual control law α_2 is chosen as

$$\alpha_2 = \frac{1}{K}\left(-k_2e_2 + Kx_1 + MgL\sin x_1 + Iz_{1\mathrm{d}} - v_1 - I\hat{d}_1\right) \tag{26}$$

where k_2 is a positive design parameter; $\hat{d}_1$ is the estimate of d_1 from the RESO (8). Subsisting (26) into (25) yields

$$\dot{V}_2 = -k_1v_1^2 - k_2v_2^2 + Kv_2v_3 - Iv_2\tilde{d}_1 \tag{27}$$

If $v_3 = 0$ and $\tilde{d}_1 = 0$, then $\dot{V}_2 \leq 0$.

Step 3: To stabilize v_3, the third Lyapunov function candidate is chosen as:

$$V_3 = V_2 + \frac{1}{2}v_3^2 \tag{28}$$

The time derivative of v_3 is computed by

$$\begin{aligned}\dot{v}_3 &= \dot{e}_3 - \dot{\xi}_3 = \dot{x}_3 - \dot{z}_2 - \dot{\xi}_3\\ &= x_4 - z_{2\mathrm{d}} - \dot{\xi}_3 = v_4 + z_3 + \xi_4 - z_{2\mathrm{d}} - \dot{\xi}_3\end{aligned} \tag{29}$$

Taking the time derivative of V_3 along (29) and using the third equation of (16) yields

$$\begin{aligned}\dot{V}_3 &= \dot{V}_2 + v_3\dot{v}_3 \\ &= -k_1v_1^2 - k_2v_2^2 + Kv_2v_3 - Iv_2\tilde{d}_1 + v_3\left(v_4 + z_3 + \dot{\xi}_4 - z_{2\mathrm{d}} - \dot{\xi}_3\right) \\ &= -k_1v_1^2 - k_2v_2^2 - Iv_2\tilde{d}_1 + v_3(Kv_2 + v_4 + \alpha_3 - z_{2\mathrm{d}} + k_3e_3 - k_3v_3)\end{aligned} \tag{30}$$

To make V_3 negative, the virtual control law α_3 is chosen as

$$\alpha_3 = -k_3e_3 + z_{2\mathrm{d}} - Kv_2 \tag{31}$$

where k_3 is a positive design parameter. Substituting (31) into (30) yields

$$\dot{V}_3 = -k_1v_1^2 - k_2v_2^2 - k_3v_3^2 + v_3v_4 - Iv_2\tilde{d}_1 \tag{32}$$

If $v_4 = 0$ and $\tilde{d}_1 = 0$, then $\dot{V}_3 \leq 0$.

Step 4: To stabilize v_4, the final Lyapunov function candidate is chosen as:

$$V_4 = V_3 + \frac{1}{2}Jv_4^2 \tag{33}$$

The time derivative of v_4 is

$$\dot{v}_4 = \dot{e}_4 - \dot{\xi}_4 = \dot{x}_4 - \dot{z}_3 - \dot{\xi}_4 = \frac{u}{J} + \frac{K}{J}(x_1 - x_3) + d_2 - z_{3\mathrm{d}} - \dot{\xi}_4 \tag{34}$$

Taking the time derivative of V_4 along (34) and using the fourth equation of (16) yields

$$\begin{aligned}\dot{V}_4 &= \dot{V}_3 + Jv_4\dot{v}_4 \\ &= -k_1v_1^2 - k_2v_2^2 - k_3v_3^2 + v_3v_4 - Iv_2\tilde{d}_1 \\ &\quad + v_4\left[u + K(x_1 - x_3) + Jd_2 - Jz_{3\mathrm{d}} - J\dot{\xi}_4\right] \\ &= -k_1v_1^2 - k_2v_2^2 - k_3v_3^2 - Iv_2\tilde{d}_1 \\ &\quad + v_4[v_3 + u + K(x_1 - x_3) + Jd_2 - Jz_{3\mathrm{d}} + k_4e_4 - k_4v_4]\end{aligned} \tag{35}$$

To make V_4 negative, the actual control law u is designed as

$$u = -k_4e_4 - K(x_1 - x_3) + Jz_{3\mathrm{d}} - v_3 - J\hat{d}_2 \tag{36}$$

where k_4 is a positive design parameter, and $\hat{d}_2$ is the estimate of d_2 from the RESO (9). Substituting (36) into (35) yields

$$\dot{V}_4 = -k_1v_1^2 - k_2v_2^2 - k_3v_3^2 - k_4v_4^2 - Iv_2\tilde{d}_1 - Jv_4\tilde{d}_2 \tag{37}$$

If $\tilde{d}_1 = 0$ and $\tilde{d}_2 = 0$, then $\dot{V}_4 \leq 0$.

Summarizing the above design steps, the proposed SCFB controller is composed of the following control laws.

$$\begin{cases} \alpha_1 = -k_1e_1 + \dot{y}_{\mathrm{d}} \\ \alpha_2 = \dfrac{1}{K}\left(-k_2e_2 + Kx_1 + MgL\sin x_1 + Iz_{1\mathrm{d}} - v_1 - I\hat{d}_1\right) \\ \alpha_3 = -k_3e_3 + z_{2\mathrm{d}} - Kv_2 \\ u = -k_4e_4 - K(x_1 - x_3) + Jz_{3\mathrm{d}} - v_3 - J\hat{d}_2 \end{cases} \tag{38}$$

where $z_{i\mathrm{d}}(i = 1, 2, 3)$ come from the SCFs (4), and $\hat{d}_1, \hat{d}_2$ are from the RESOs (8) and (9). The block diagram of the proposed RESO based SCFB composite control system for the single-link FJM is shown in Figure 3.

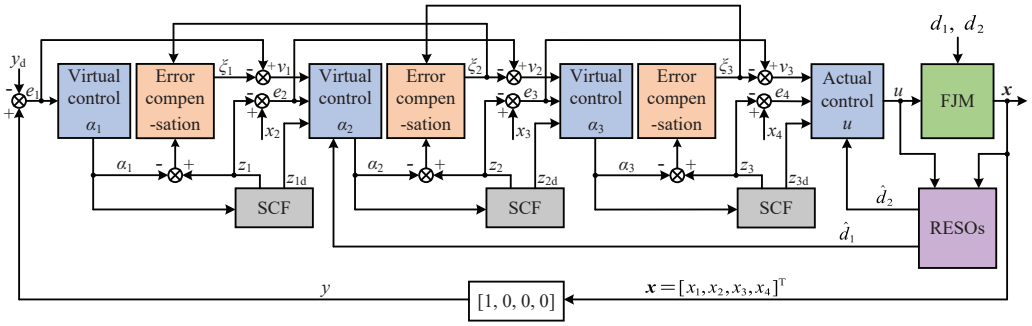

Figure 3. Block diagram of the composite control system for the single–link FJM control system.

4. Stability Analysis

In this section, the convergence of the error signals and the stability of the resulting control system are analyzed using the Lyapunov stability theory.

Theorem 1. *Consider the proposed RESOs (8) and (9) for the single-link FJM described by (2) with matched and mismatched disturbances. If Assumption 2 is satisfied, then the error norm of the RESOs is bounded by*

$$\|\boldsymbol{e}_o\| \leq \frac{\max(\bar{d}_i)}{\min(|\beta_i|)}(i=1,2) \tag{39}$$

Proof. Consider the Lyapunov function candidate V_o

$$V_o = \frac{1}{2}\boldsymbol{e}_o^{\top}\boldsymbol{P}\boldsymbol{e}_o \tag{40}$$

where $\boldsymbol{P}$ is a positive definite matrix. Since $\boldsymbol{A}_o$ is a Hurwitz matrix, there exists a positive definite matrix $\boldsymbol{Q}$ such that

$$\boldsymbol{A}_o^{\top}\boldsymbol{P} + \boldsymbol{P}\boldsymbol{A}_o = -\boldsymbol{Q} \tag{41}$$

Taking the time derivative of V_o along (14) and (41) yields

$$\begin{aligned}
\dot{V}_o &= \frac{1}{2}\dot{\boldsymbol{e}}_o^{\mathrm{T}}\boldsymbol{P}\boldsymbol{e}_o + \frac{1}{2}\boldsymbol{e}_o^{\mathrm{T}}\boldsymbol{P}\dot{\boldsymbol{e}}_o \\
&= \frac{1}{2}\boldsymbol{e}_o^{\mathrm{T}}\left(\boldsymbol{A}_o^{\mathrm{T}}\boldsymbol{P} + \boldsymbol{P}\boldsymbol{A}_o\right)\boldsymbol{e}_o + \boldsymbol{e}_o^{\mathrm{T}}\boldsymbol{P}\dot{\boldsymbol{d}} \\
&= -\frac{1}{2}\boldsymbol{e}_o^{\mathrm{T}}\boldsymbol{Q}\boldsymbol{e}_o + \boldsymbol{e}_o^{\mathrm{T}}\boldsymbol{P}\dot{\boldsymbol{d}} \\
&\leq -\frac{1}{2}\|\boldsymbol{e}_o\|^2\boldsymbol{Q} + \|\boldsymbol{e}_o\|\|\boldsymbol{P}\|\max(\bar{d}_i) \\
&\leq -\|\boldsymbol{e}_o\|\left[\|\boldsymbol{e}_o\|\|\boldsymbol{P}\|\min(|\beta_i|) - \|\boldsymbol{P}\|\max(\bar{d}_i)\right]
\end{aligned} \tag{42}$$

where $\min(|\beta_i|)(i=1,2)$ represents the smallest eigenvalue of $\boldsymbol{A}_o$. Therefore, within finite time, the norm of the estimation errors is bounded by

$$\|\boldsymbol{e}_o\| \leq \frac{\max(\bar{d}_i)}{\min(|\beta_i|)}(i=1,2) \tag{43}$$

This completes the proof of Theorem 1. □

Theorem 2. *Consider the single-link FJM described by (2) with matched and mismatched disturbances. Suppose that Assumptions 1 and 2 are satisfied. The RESOs (8) and (9), the error compensation system (16), and the SCFB controller (38) guarantee that all the signals in the control system are uniformly ultimately bounded, and the tracking errors converge to a small neighborhood around zero.*

Proof. Based on the design procedure in Section 3.2, the final Lyapunov function candidate for the feedback control is

$$V_f = \frac{1}{2}v_1^2 + \frac{I}{2}v_2^2 + \frac{1}{2}v_3^2 + \frac{J}{2}v_4^2 \tag{44}$$

According to (37), the time derivative of V_f can be described as

$$\dot{V}_f = -k_1 v_1^2 - k_2 v_2^2 - k_3 v_3^2 - k_4 v_4^2 - I v_2 \tilde{d}_1 - J v_4 \tilde{d}_2 \tag{45}$$

Using the Young's inequality, we have

$$\begin{aligned} \left| I v_2 \tilde{d}_1 \right| &\leq \frac{I}{2} v_2^2 + \frac{I}{2} \tilde{d}_1^2 \\ \left| J v_4 \tilde{d}_2 \right| &\leq \frac{J}{2} v_4^2 + \frac{J}{2} \tilde{d}_2^2 \end{aligned} \tag{46}$$

Substituting (46) into (45) yields

$$\dot{V}_f \leq -k_1 v_1^2 - \left(k_2 - \frac{I}{2} \right) v_2^2 - k_3 v_3^2 - \left(k_4 - \frac{J}{2} \right) v_4^2 - \frac{I}{2} \tilde{d}_1^2 - \frac{J}{2} \tilde{d}_2^2 \tag{47}$$

Rewriting inequality (47) in a compact form, we have

$$\dot{V}_f \leq -\alpha_0 V_f + D \tag{48}$$

where

$$\begin{aligned} \alpha_0 &= \min \left(2k_1, 2k_2 - I, 2k_3, 2k_4 - J \right) \\ D &= -\frac{I}{2} \tilde{d}_1^2 - \frac{J}{2} \tilde{d}_2^2 \end{aligned} \tag{49}$$

Selecting the design parameters $k_1 > 0, k_2 > I/2, k_3 > 0, k_4 > J/2$ to ensure $\alpha_0 > 0$. Then, according to Lemma 2, the solution of (48) is

$$V_f(t) \leq \frac{D}{\alpha_0} + \left[V_f(0) - \frac{D}{\alpha_0} \right] e^{-\alpha_0 t} \tag{50}$$

which means that $V_f(t)$ converges exponentially to the upper bound of $\frac{D}{\alpha_0}$, i.e., as $t \to \infty$, $V_f(t) \leq \frac{D}{\alpha_0}$. As a result, the compensated errors $v_i (i = 1, 2, 3, 4)$ are bounded.

Furthermore, it has been proved in Ref. [50] that the compensation signals $\xi_i (i = 1, 2, 3, 4)$ in (16) are bounded. Since $e_i = v_i + \xi_i$, it is clearly known that the tracking errors e_i are also bounded. According to Lemma 1 and Theorem 1, the filter outputs $z_i, z_{i\mathrm{d}} (i = 1, 2, 3)$ and the estimations $\hat{d}_1, \hat{d}_2$ are bounded. From (38), it is evident that the virtual control laws $\alpha_1(\dot{x}_\mathrm{d}, e_1)$, $\alpha_2\left(x_1, e_2, \hat{d}_1, z_{1\mathrm{d}}, v_1\right)$, $\alpha_3(e_3, z_{2\mathrm{d}}, v_2)$, and the actual law $u\left(x_1, x_3, e_4, \hat{d}_2, z_{3\mathrm{d}}, v_3\right)$ are also bounded because of the boundedness of their independent variables.

Therefore, all the signals in the closed-loop control system are uniformly ultimately bounded. In addition, by properly choosing the design parameters, such as large k_i(i=1,2,3,4) and $\beta_i (i = 1, 2)$, the tracking errors $e_i (i = 1, 2, 3, 4)$ can converge to a small neighbourhood around zero. This completes the proof of Theorem 2. □

5. Numerical Simulations

To evaluate the effectiveness and efficiency of the proposed control method, two simulation tests are conducted in the MATLAB/SIMULINK platform. Specifically, the first simulation is presented to examine the tracking control performance of the proposed approach for the single-link FJM with matched and mismatched disturbances as well as measurement noises. In the second simulation, a comparison study between the proposed method and the existing approaches are presented to show the superior performance of the proposed controller.

The physical parameters of the single-link FJM in (1) are given as: $M = 0.25$ kg, $g = 9.8$ m/s^2, $L = 0.45$ m, $K = 5$ N $\cdot$ m/rad, $I = 0.05$ m/s^2, $J = 0.0005$ m/s^2. The gains of the controller (38) are chosen as $k_1 = 7, k_2 = 25, k_3 = 8, k_4 = 8$. Meanwhile, the parameters of the SCFs (4) are chosen as $\omega_n = 1100$, $\zeta = 0.8$, and the parameters of the proposed RESOs in (8) and (9) are: $\beta_1 = 50, \beta_2 = 50$.

The initial condition of the FJM is set as $x(0) = [0.5, 0, 0, 0]^\top$. The initial states of the error compensation system and the SCFs are all zeros. The desired reference trajectory is chosen as $y_\mathrm{d} = 0.5(\sin t + \sin 0.5t)$, and the lumped mismatched and matched disturbances added for the two simulations are given as:

$$\begin{cases} w_1 = 0.005\cos\dot{q} + 0.3\sin(2\pi t) \\ w_2 = 0.1\dot{\theta} + 0.3\cos(2\pi t) \end{cases} \tag{51}$$

5.1. Simulation Results with Disturbances and Noises

To imitate the measurement noises of encoders equipped in the FJM, Gaussian white noise with zero mean and standard deviation of 0.1, which can be generated by the "randn" function in MATLAB, is added for all the state measurements. The simulation results are depicted in Figures 4–9.

Figure 4 displays the trajectories of the system output y and the given reference signal y_d. Figure 5 shows the curve of tracking error. From these figures, we can see that the proposed approach achieves a satisfactory tracking control performance despite the presence of mismatched and matched disturbances as well as noises affecting measurements. The estimates of the mismatched and matched disturbances are respectively illustrated in Figures 6 and 7, from which we can see that the designed RESOs can estimate the disturbances quickly and precisely.

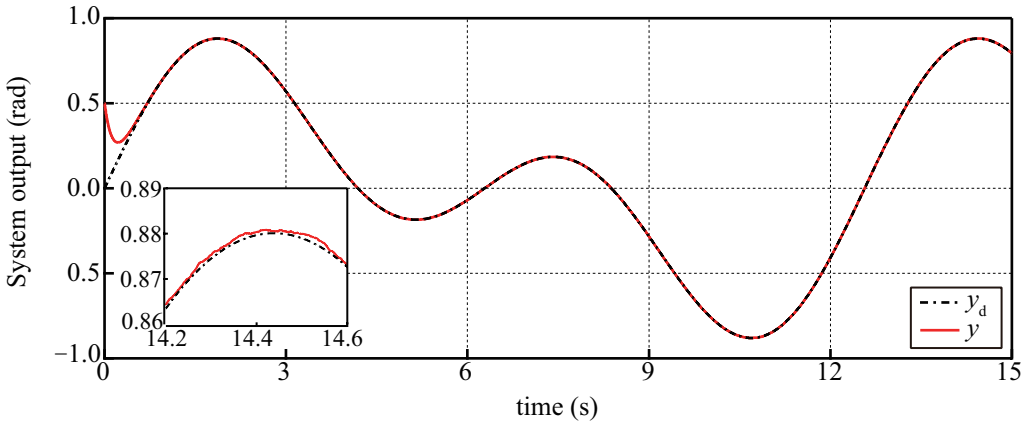

Figure 4. Tracking performance of the system output y under the proposed approach with noises.

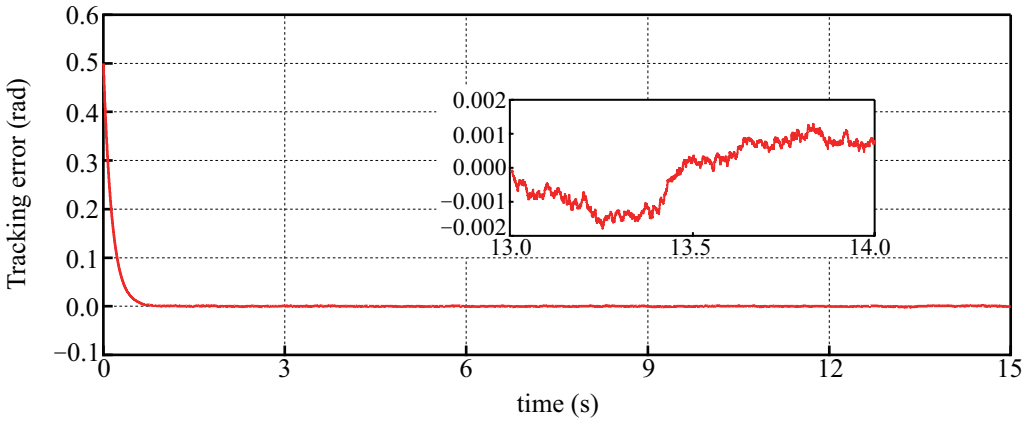

Figure 5. Tracking error e_1 under the proposed approach with noises.

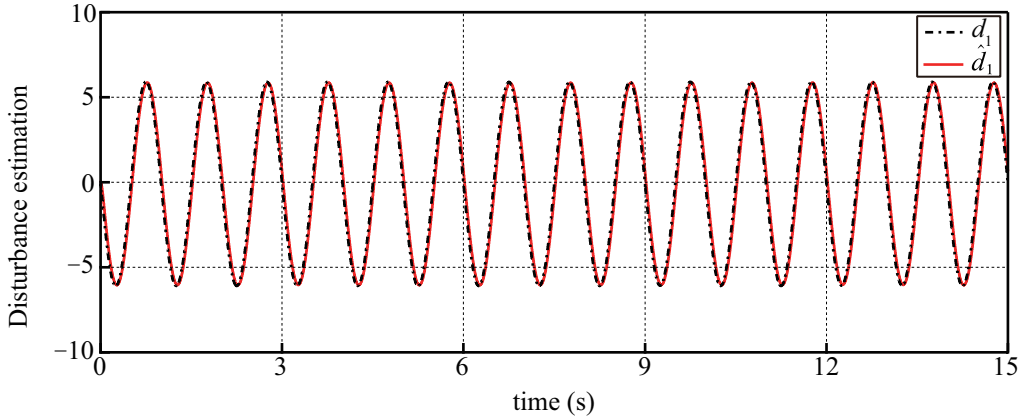

Figure 6. Estimation performance of d_1 via RESO.

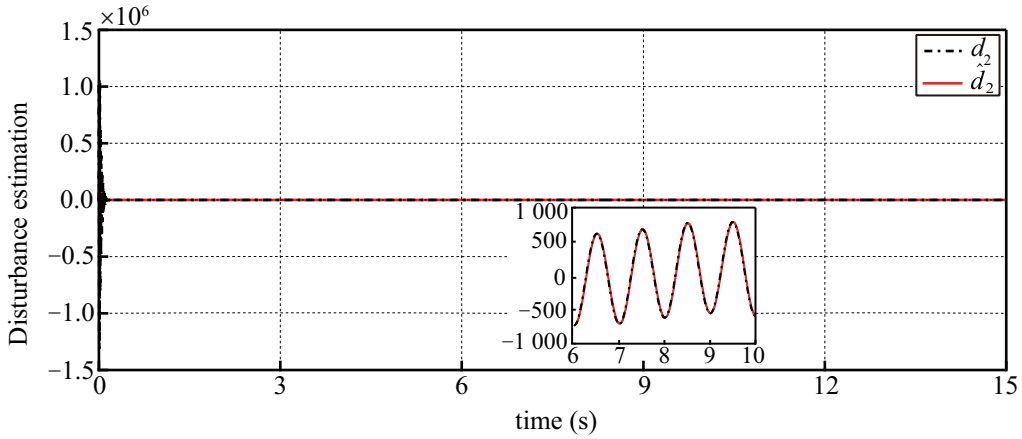

Figure 7. Estimation performance of d_2 via RESO.

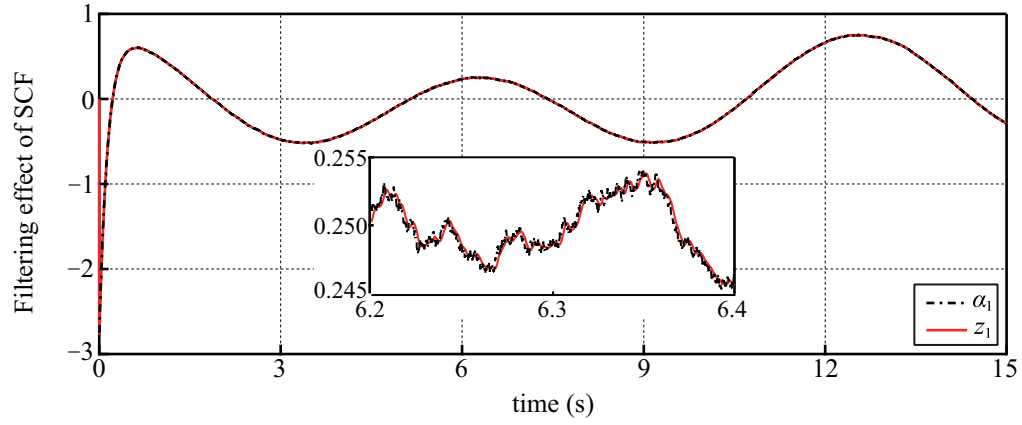

Figure 8. Filtering performance of the SCF with α_1 being the input and z_1 being the output.

Figure 8 depicts the intermediate virtual control law α_1 and the corresponding filtered control signal z_1 from the SCF. It is clearly seen that the virtual control law α_1 is corrupted by the white noises, but the filtered signal z_1 through the SCF is smooth. In addition, Figure 9 shows the comparison results between the direct time derivative of α_1 and the output z_{1d} of the SCF in the presence of white noises. It is noticed that the chattering amplitude of $\dot{\alpha}_1$ is much bigger than that of z_{1d}, which indicates that the noises in $\dot{\alpha}_1$ are amplified. The reason is that the derivative of α_1 is approximated by the SCF through integration rather than differentiation (as shown in Figure 2). These results demonstrate that the SCF employed for FJMs with measurement noises can not only filter the noises for the control signal to some extent, but also avoid the amplification of the noises in the

recursive backstepping design. Similar results are obtained for α_i $(i = 2, 3)$ and z_{id}, which are omitted for the space saving.

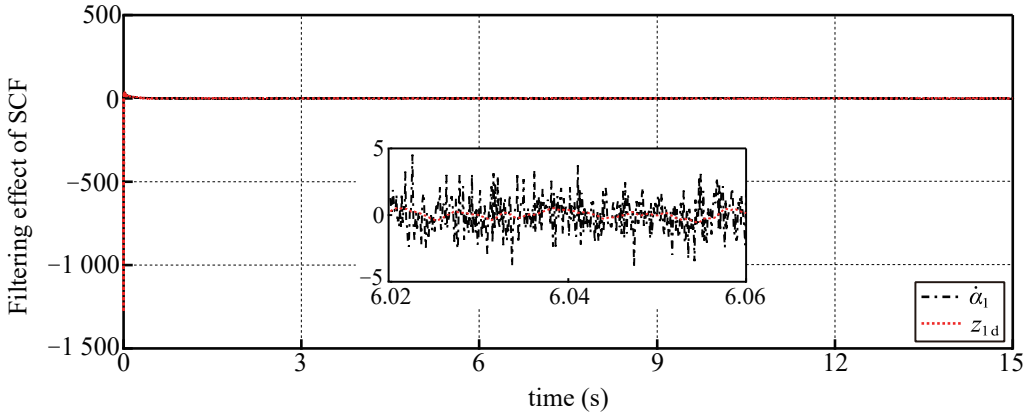

Figure 9. Comparison results between $\dot{\alpha}_1$ and the output of the SCF z_{1d}.

5.2. Comparison Results with CBC and AFCFC Methods

In order to further show the superior performance of the proposed RESO based command filtered controller (RBCFC), the following two controllers are selected to make a comparison study.

(1) **Conventional backstepping controller (CBC) proposed in [16].** The structure of the controller is given as:

$$\begin{cases} \alpha_1 = -k_1 e_1 + \dot{y}_d \\ \alpha_2 = \dfrac{1}{K}(-k_2 e_2 - e_1 + MgL \sin x_1 + Kx_1 + I\dot{\alpha}_1) \\ \alpha_3 = -k_3 e_3 - Ke_2 + \dot{\alpha}_2 \\ u = -k_4 e_4 - e_3 - K(x_1 - x_3) + J\dot{\alpha}_3 \end{cases} \tag{52}$$

(2) **Adaptive fuzzy command filtered controller (AFCFC) proposed in [30].** The structure of the controller is given as:

$$\begin{cases} \alpha_1 = -k_1 e_1 + \dot{y}_d \\ \alpha_2 = \dfrac{1}{M^{-1}K}(-k_2 e_2 - \dfrac{1}{2}v_2 - e_1 + z_{1d} - \dfrac{v_2 \hat{\theta} \psi_1^\top \psi_1}{2l_1^2}) \\ \alpha_3 = -k_3 e_3 - M^{-1} K e_2 + z_{2d} \\ u = B(e_4 + z_3) + K(e_3 + z_2 - e_1 - y_d) + J(-k_4 e_4 - e_3 + z_{3d}) \\ \dot{\hat{\theta}} = \dfrac{r v_2^\top v_2 \psi_1^\top \psi_1}{2l_1^2} - \bar{r}\hat{\theta} \end{cases} \tag{53}$$

where $z_{id}(i = 1, 2, 3)$ are the outputs of SCFs, $l_1, r, \bar{r}$ are positive design parameters, $\hat{\theta}$ is the estimation of the adaptive parameter θ, ψ_1 is the vector of fuzzy basis functions. More details about these control parameters are referred to in Ref. [30].

Remark 1. *It is noticed that the structure of the CBC is the simplest among the three controllers, but it suffers from the drawback of computational complexity, and does not consider the influence of disturbances. Both the proposed RBCFC and AFCFC can address these problems, but the AFCFC employs a fuzzy system with an online adaptive learning law to approximate the unknown disturbances, while the proposed RBCFC utilizes two simple RESOs to estimate the disturbances.*

Since the three controllers are designed using the same backstepping methodology, their gains are chosen as the same for the sake of fair comparison, i.e., $k_1 = 7$, $k_2 = 25$, $k_3 = 8$, $k_4 = 8$. Meanwhile, the same parameters of the SCFs are chosen for the proposed

controller and the AFCFC, i.e., $\omega_n = 1100$, $\zeta = 0.8$. Other parameters for the AFCFC are chosen as in Ref. [30]. No measurement noises are considered in this circumstance for a clear and fair comparison.

The simulation results of the single-link FJM under the three controllers are depicted in Figures 10–13, which record the curves of the tracking performance of the system output y, the tracking error e_1, the state of the motor angle θ, and the control torque u, respectively.

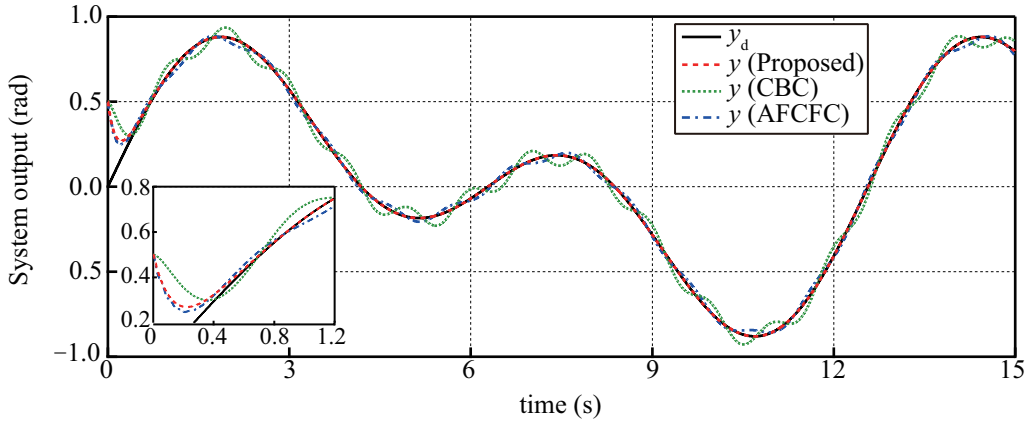

Figure 10. Tracking performance of the system output y under the three controllers.

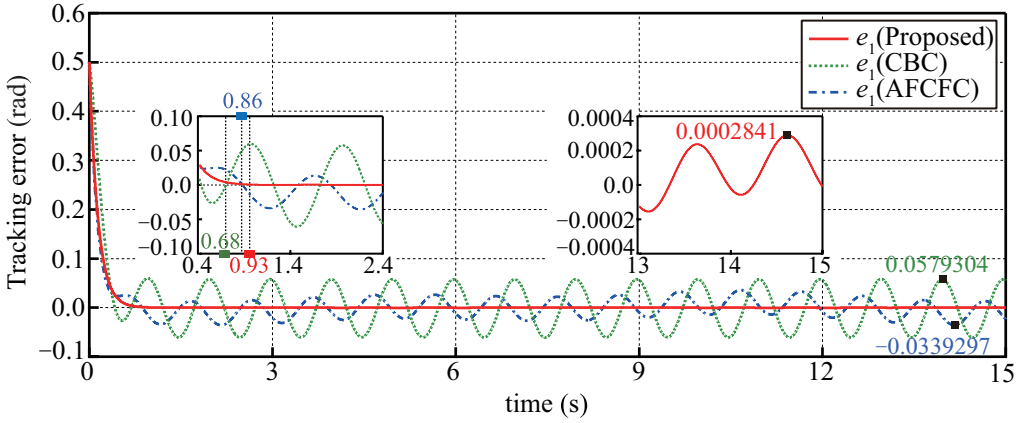

Figure 11. Tracking error e_1 under the three controllers.

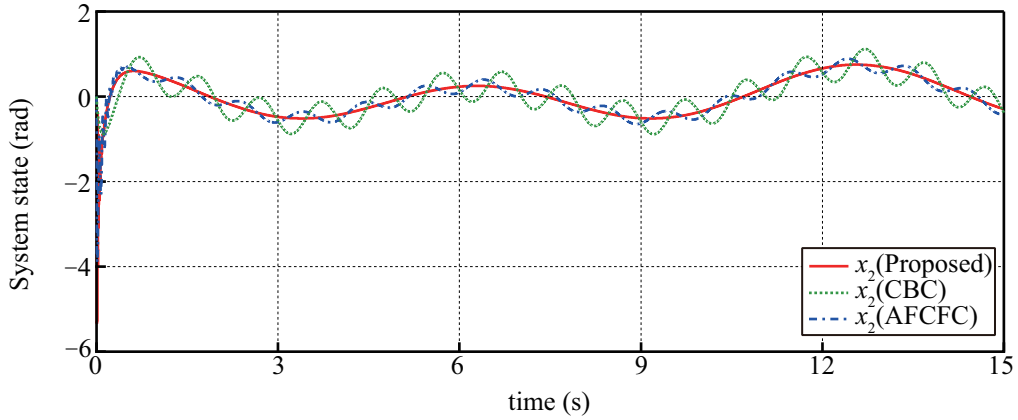

Figure 12. System state x_2 (the motor angle θ) under the three controllers.

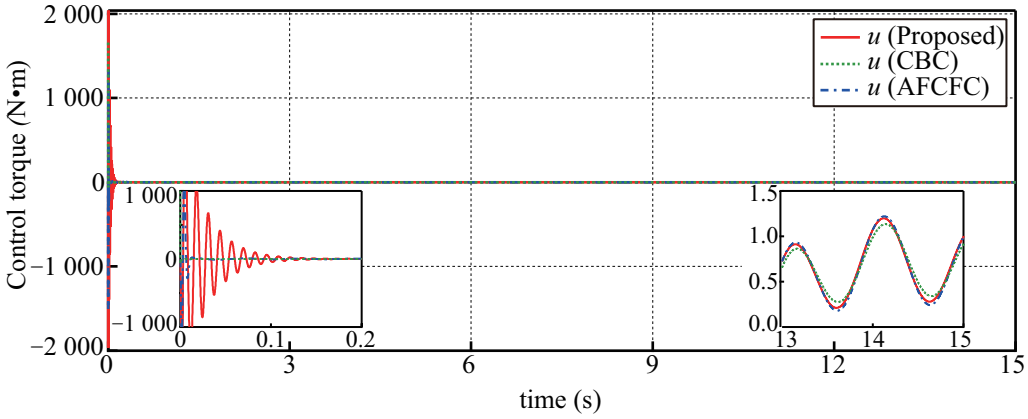

Figure 13. Control torque u under the three controllers.

From Figure 10, it is seen that both the proposed controller and the AFCFC can attenuate the influence of lumped disturbances and achieve satisfactory control performance. However, the system output with the CBC is seriously affected by the disturbances, and fluctuates around the reference trajectory. This is mainly because the CBC does not contain a compensation term for the disturbances. The same results can be further verified by Figures 11 and 12, which respectively show that the tracking error e_1 and the motor angle θ under the three controllers converge to a small neighborhood around zero. It is clearly seen that the convergence radius of the proposed controller is the smallest among the three controllers.

In order to quantitatively analyze the control performance of the three controllers, we define three performance indexes including the settling time t_s, the mean squared error in the transient stage between 0.4 s and 2.4 s, i.e.,

$$e_{1\mathrm{MSE}} = \frac{1}{N}\sum_{i=1}^{N}[e(i)]^2 \tag{54}$$

and the maximum tracking error in the steady stage $|e_{1\infty\max}|$. The details of the quantified performance indexes of the three controllers are given in Table 1.

Table 1. Performance indexes under the three controllers.

Methods	t_s (s)	$e_{1\mathrm{MSE}}$ (rad)	$\lvert e_{1\infty\max}\rvert$ (rad)
RBCFC [Proposed]	0.93	3.09×10^{-5}	2.84×10^{-4}
CBC [16]	0.68	1.51×10^{-3}	5.79×10^{-2}
AFCFC [30]	0.86	4.84×10^{-4}	3.39×10^{-2}

As seen from Table 1, the proposed RBCFC exhibits better performance than the other two controllers in aspects of transient and steady tracking errors. Although the settling time of the proposed controller is a little longer than those of other controllers, the mean squared error of the proposed controller in the transient stage is reduced almost down to 3.09×10^{-5}, which is quite smaller than that (i.e., 1.51×10^{-3}) of CBC, as well as that (i.e., 4.84×10^{-4}) of AFCFC. In addition, the maximum tracking error of the proposed controller in the steady stage is about 2.84×10^{-4}, while those of CBC and AFCFC are 5.79×10^{-2} and 3.39×10^{-2}, respectively. Compared with the CBC and the AFCFC, the tracking accuracy of the proposed controller is improved by 99.5% and 99.2%, respectively.

From Figure 13, it is seen that the control torque u of the proposed controller in the initial stage between 0 s and 0.2 s shows large fluctuations. The reason for this may be that the proposed controller in the system adjustment stage is more susceptible to the unknown disturbances. By introducing the RESOs, however, the disturbances are quickly estimated and compensated for in the feedback control.

According to the above comparative simulation results, it can be concluded that compared with other methods, the proposed controller can estimate and compensate the unknown matched and mismatched disturbances effectively, and achieve a better transient and steady tracking performance.

6. Conclusions

This paper has successfully proposed an efficient model-assisted composite control approach for the high precision tracking control of FJMs in the presence of lumped matched and mismatched disturbances. Two RESOs are constructed with partial known model information of FJMs to estimate and compensate the disturbances, three second-order command filters are incorporated into the backstepping control design to avoid the problem of "explosion of complexity", and an error compensation dynamic system is designed to reduce the filtering errors. The stability of the resulting control system is rigorously proven via Lyapunov stability theory, and the tracking errors are guaranteed to be uniformly ultimately bounded. The numerical simulation results prove that the proposed RESOs deliver accurate estimates of both the matched and mismatched disturbances. In addition, compared with conventional backstepping method and adaptive fuzzy command filtered control method, the proposed approach achieves a better tracking performance, i.e., the tracking accuracy is improved by 99.5% and 99.2%, respectively.

It is worth pointing out that the proposed approach requires the knowledge of all the state variables, which may be unfeasible or inconvenient in practice. It is interesting to study the output feedback control problem of FJMs with unmeasured state variables by integrating the state estimation technique, e.g., Kalman state observers presented in Refs. [1,2]. In addition, it is necessary and significant to evaluate the control performance of the proposed approach under varying load mass and extend the proposed approach to a more general 6-DOF FJM. These issues will be investigated in our future works.

Author Contributions: Conceptualization, C.P. and X.F.; methodology, X.F.; software, X.F. and Z.L.; validation, C.P., X.F. and H.H.; formal analysis, Z.L.; investigation, C.P. and X.F.; resources, C.P., X.F. and H.H.; data curation, X.F.; writing—original draft preparation, X.F.; writing—review and editing, C.P. and J.X.; visualization, P.X. and Z.L.; supervision, C.P.; project administration, C.P. and J.X.; funding acquisition, C.P. and J.X. All authors have read and agreed to the published version of the manuscript.

Funding: This work is supported in part by: (i) National Natural Science Foundation of China (Grant No. 62173138); (ii) Guangdong Basic and Applied Basic Research Foundation (Grant Nos. 2020A1515011082 and 2019A1515010955); (iii) Scientific Research Fund of Hunan Provincial Education Department (Grant Nos. 20A186 and 21C0329); (iv) Hunan Provincial Natural Science Foundation of China (Grant No. 2022JJ30263).

Institutional Review Board Statement: Not applicable.

Informed Consent Statement: Not applicable.

Data Availability Statement: Not applicable.

Conflicts of Interest: The authors declare no conflict of interest.

References

1. Barjuei, E.S.; Gasparetto, A. Predictive control of spatial flexible mechanisms. *Int. J. Mech. Control* **2015**, *16*, 85–96.
2. Palomba, I.; Richiedei, D.; Trevisani, A. Reduced-order observers for nonlinear state estimation in flexible multibody systems. *Shock Vib.* **2018**, *2018*, 6538737. [CrossRef]
3. Zhang, A.; Lin, Z.; Wang, B.; Han Z. Nonlinear model predictive control of single-link flexible-joint robot using recurrent neural network and differential evolution optimization. *Electronics* **2021**, *10*, 2426. [CrossRef]
4. Spyrakos-Papastavridis, E.; Da, J.S. Minimally model-based trajectory tracking and variable impedance control of flexible-joint robots. *IEEE Trans. Ind. Electron.* **2020**, *68*, 6031–6041. [CrossRef]
5. Li, Z.; Yang, C.; Su, C.Y.; Deng, A.; Fuchun, S.; Sun, F.; Zhang, W. Decentralized fuzzy control of multiple cooperating robotic manipulators with impedance interaction. *IEEE Trans. Fuzzy Syst.* **2014**, *23*, 1044–1056. [CrossRef]

6. Chen, T.; Shan, J. Distributed control of multiple flexible manipulators with unknown disturbances and dead-zone input. *IEEE Trans. Ind. Electron.* **2019**, *67*, 9937–9947. [CrossRef]
7. Yang, C.; Jiang, Y.; He, W.; Na, J.; Li, Z.; Xu, B. Adaptive parameter estimation and control design for robot manipulators with finite-time convergence. *IEEE Trans. Ind. Electron.* **2018**, *65*, 8112–8123. [CrossRef]
8. Ibrahim, K.; Sharkawy, A.B. A hybrid PID control scheme for flexible joint manipulators and a comparison with sliding mode control. *Ain Shams Eng. J.* **2018**, *9*, 3451–3457. [CrossRef]
9. Kelekci, E.; Kizir, S. Trajectory and vibration control of a flexible joint manipulator using interval type-2 fuzzy logic. *ISA Trans.* **2019**, *94*, 218–233. [CrossRef]
10. Ak, A. Sliding mode controller design using fuzzy sliding surface for flexible joint manipulator. *IETE J. Res.* **2021**, *68*, 760–767. [CrossRef]
11. Sun, T.; Liang, D.; Song, Y. Singular-perturbation-based nonlinear hybrid control of redundant parallel robot. *IEEE Trans. Ind. Electron.* **2017**, *65*, 3326–3336. [CrossRef]
12. Chen, H.; Dong, X.; Yang, Y.; Liu, J. Backstepping sliding mode control of uncertainty flexible joint manipulator with actuator saturation. In Proceedings of the 2020 International Symposium on Automation, Information and Computing, Beijing, China, 2–4 December 2020; Volume 1828.
13. Hooshmand, H.; Fateh, M.M. Voltage control of flexible-joint robot manipulators using singular perturbation technique for model order reduction. *J. Electr. Comput. Eng. Innov.* **2022**, *10*, 123–142.
14. Korayem, M.H.; Nekoo, S.R.; Kazemi, S. Finite-time feedback linearization (FTFL) controller considering optimal gains on mobile mechanical manipulators. *J. Intell. Robot. Syst.* **2019**, *94*, 727–744. [CrossRef]
15. Abdul-Adheem, W.R.; Ibraheem, I.K.; Humaidi, A.J.; Azar, A.T. Model-free active input–output feedback linearization of a single-link flexible joint manipulator: An improved active disturbance rejection control approach. *Meas. Control* **2021**, *54*, 856–871. [CrossRef]
16. Oh, J.H.; Lee, J.S. Control of flexible joint robot system by backstepping design approach. *Intell. Autom. Soft Comput.* **1999**, *5*, 267–278. [CrossRef]
17. Huang, A.C.; Chen, Y.C. Adaptive sliding control for single-link flexible-joint robot with mismatched uncertainties. *IEEE Trans. Control Syst. Technol.* **2004**, *12*, 770–775. [CrossRef]
18. Dian, S.; Hu, Y.; Zhao, T.; Han, J. Adaptive backstepping control for flexible-joint manipulator using interval type-2 fuzzy neural network approximator. *Nonlinear Dyn.* **2019**, *97*, 1567–1580. [CrossRef]
19. Wang, L.; Shi, Q.; Liu, J.; Zhang, D. Backstepping control of flexible joint manipulator based on hyperbolic tangent function with control input and rate constraints. *Asian J. Control* **2020**, *22*, 1268–1279. [CrossRef]
20. Swaroop, D.; Hedrick, J.K.; Yip, P.P.; Gerdes, J.C. Dynamic surface control for a class of nonlinear systems. *IEEE Trans. Aautomatic Control* **2000**, *45*, 1893–1899. [CrossRef]
21. Ling, S.; Wang, H.; Liu, P.X. Adaptive fuzzy dynamic surface control of flexible-joint robot systems with input saturation. *IEEE/CAA J. Autom. Sin.* **2019**, *6*, 97–107. [CrossRef]
22. Yoo, S.J.; Park, J.B.; Choi, Y.H. Adaptive output feedback control of flexible-joint robots using neural networks: Dynamic surface design approach. *IEEE Trans. Neural Netw.* **2008**, *19*, 1712–1726. [PubMed]
23. Li, Y.; Tong, S.; Li, T. Fuzzy adaptive dynamic surface control for a single-link flexible-joint robot. *Nonlinear Dyn.* **2012**, *70*, 2035–2048. [CrossRef]
24. Xiong, G.; Xie, Z.; Huang, J.; Liu, H.; Jiang, Z.; Sun, K. Dynamic surface control-backstepping based impedance control for 5-DOF flexible joint robots. *J. Cent. South Univ. Technol.* **2010**, *17*, 807–815. [CrossRef]
25. Farrell, J.A.; Polycarpou, M.; Sharma, M.; Dong, W. Command filtered backstepping. *IEEE Trans. Autom. Control* **2009**, *54*, 1391–1395. [CrossRef]
26. Dong, W.; Farrell, J.A.; Polycarpou, M.M.; Djapic, V.; Sharma, M. Command filtered adaptive backstepping. *IEEE Trans. Control Syst. Technol.* **2012**, *20*, 566–580. [CrossRef]
27. Wang, L.; Yang, C. Neural network adaptive command filtered control of robotic manipulators with input saturation. *Int. J. Adv. Robot. Syst.* **2019**, *16*, 1729881419894779. [CrossRef]
28. Deng, Y. Adaptive finite-time fuzzy command filtered controller design for uncertain robotic manipulators. *Int. J. Adv. Robot. Syst.* **2019**, *16*, 1729881419828148. [CrossRef]
29. Lin, M.; Lei, Z.; Zhang, Y.; Li, P.; Wang, X. Command filter backstepping control with error compensation for flexible-joint manipulator. In Proceedings of the 2020 Chinese Control And Decision Conference, Hefei, China, 22–24 August 2020; pp. 3696–3701.
30. Ling, S.; Wang, H.; Liu, P.X. Adaptive fuzzy tracking control of flexible-joint robots based on command filtering. *IEEE Trans. Ind. Electron.* **2019**, *67*, 4046–4055. [CrossRef]
31. Liu, X.; Yang, C.; Chen, Z.; Wang, M.; Su, C. Neuro-adaptive observer based control of flexible joint robot. *Neurocomputing* **2018**, *275*, 73–82. [CrossRef]
32. Sun, W.; Su, S.F.; Xia, J.; Nguyen, V. Adaptive fuzzy tracking control of flexible-joint robots with full-state constraints. *IEEE Trans. Syst. Man Cybern. Syst.* **2018**, *49*, 2201–2209. [CrossRef]
33. Soltanpour, M.R.; Moattari, M. Voltage based sliding mode control of flexible joint robot manipulators in presence of uncertainties. *Robot. Auton. Syst.* **2019**, *118*, 204–219.

34. Cheng, X.; Liu, H.; Lu, W. Chattering-suppressed sliding mode control for flexible-joint robot manipulators. *Actuators Multidiscip. Digit. Publ. Inst.* **2021**, *10*, 288. [CrossRef]
35. Alam, W.; Ahmad, S.; Mehmood, A.; Iqbal, J. Robust sliding mode control for flexible joint robotic manipulator via disturbance observer. *Interdiscip. Descr. Complex Syst. INDECS* **2019**, *17*, 85–97. [CrossRef]
36. Zaare, S.; Soltanpour, M.R. Continuous fuzzy nonsingular terminal sliding mode control of flexible joints robot manipulators based on nonlinear finite time observer in the presence of matched and mismatched uncertainties. *J. Frankl. Inst.* **2020**, *357*, 6539–6570. [CrossRef]
37. Ullah, H.; Malik, F.M.; Raza, A.; Mazhar, N.; Khan, R.; Saeed, A.; Ahmad, I. Robust output feedback control of single-link flexible-joint robot manipulator with matched disturbances using high gain observer. *Sensors* **2021**, *21*, 3252. [CrossRef]
38. Hu, Y.; Dian, S.; Guo, R.; Li, S.; Zhao, T. Observer-based dynamic surface control for flexible-joint manipulator system with input saturation and unknown disturbance using type-2 fuzzy neural network. *Neurocomputing* **2021**, *436*, 162–173. [CrossRef]
39. Han, J.Q. From PID to active disturbance rejection control. *IEEE Trans. Ind. Electron.* **2009**, *56*, 900–906. [CrossRef]
40. Talole, S.E.; Kolhe, J.P.; Phadke, S.B. Extended-state-observer-based control of flexible-joint system with experimental validation. *IEEE Trans. Ind. Electron.* **2009**, *57*, 1411–1419. [CrossRef]
41. Rsetam, K.; Cao, Z.; Man, Z. Cascaded-extended-state-observer-based sliding-mode control for underactuated flexible joint robot. *IEEE Trans. Ind. Electron.* **2019**, *67*, 10822–10832. [CrossRef]
42. Huang, Y.; Xue, W. Active disturbance rejection control: Methodology and theoretical analysis. *ISA Trans.* **2014**, *53*, 963–976. [CrossRef]
43. Shao, X.; Wang, H. Back-stepping active disturbance rejection control design for integrated missile guidance and control system via reduced-order ESO. *ISA Trans.* **2015**, *57*, 10–22.
44. Zhou, Y.; Chang, S. A model-assisted reduced-order ESO based cascade controller for sensorless control of independent gear-shifting actuators. *Appl. Sci.* **2017**, *7*, 1283. [CrossRef]
45. Xie, T.; Li, Y.; Jiang, Y.; An, L.; Wu, H. Backstepping active disturbance rejection control for trajectory tracking of underactuated autonomous underwater vehicles with position error constraint. *Int. J. Adv. Robot. Syst.* **2020**, *17*, 1–12. [CrossRef]
46. Wang, J.; Rong, J.; Yu, L. Reduced-order extended state observer based event-triggered sliding mode control for DC-DC buck converter system with parameter perturbation. *Asian J. Control* **2021**, *23*, 1591–1601. [CrossRef]
47. Zhai, J.; Li, S.; Xu, Z.; Zhang, L.; Li, J. Reduced-order extended state observer-based sliding mode control for all-clamped plate using an inertial actuator. *Energies* **2022**, *15*, 1780. [CrossRef]
48. Chien, M.C.; Huang, A.C. Adaptive control for flexible-joint electrically driven robot with time-varying uncertainties. *IEEE Trans. Ind. Electron.* **2007**, *54*, 1032–1038. [CrossRef]
49. Narendra, K.S.; Annaswamy, A.M. *Robust Adaptive Control. Adaptive and Learning Systems*; Springer: Boston, MA, USA, 1986; pp. 3–31.
50. Yu, J.; Shi, P.; Dong, W.; Yu, H. Observer and command-filter-based adaptive fuzzy output feedback control of uncertain nonlinear systems. *IEEE Trans. Ind. Electron.* **2015**, *62*, 5962–5970. [CrossRef]